The Shape of Dark Matter Halos in a ΛCDM Cosmology

Senior Thesis

Samuel Kahn

Advisor: Joel R. Primack

University of California at Santa Cruz

October 12, 2013

Contents

Abstract

We use the Bolshoi and Multidark Simulations to study the statistics of dark matter halo concentrations and shapes in a Λ Cold Dark Matter (ΛCDM) cosmology. Our analysis spans the mass range $(6.3 \cdot 10^{10} - 3.2 \cdot 10^{15})h^{-1}M_{\odot}$ and z=0–6. We define concentration with two different scale radii by fitting an NFW (Navarro-Frenk-White 1997) profile and using a method presented in Prada et al. 2011, finding the average concentration systematically lower by fitting NFW. Our results agree with previous results (Neto et al 2007, Prada et al. 2011, Ludlow et al. 2012) that halo concentration declines monotonically for z=0-1 and exhibits an upturn in the high mass range. For z=2-6 our results for average concentration start flat and display a rapid upturn in agreement with Prada et al. 2011. We impose relaxation criteria on our halos to reduce our sample to halos in dynamical equilibrium. We observe an increase in concentration from z=0-2 and an upturn for z=0-1, which is at odds with Neto et al. 2007 and Ludlow et al. 2012. We present results for the median halo shape using algorithms presented by Allgood et al. 2006 and Zemp et al. 2011 at R_{vir} and $0.3R_{vir}$.

1 Introduction

1.1 A Brief Preamble

1.1.1 Cosmology

Physical cosmology seeks to understand the evolution, origin, and fate of the universe and explain the natural processes that arrange our universe the way it is today. The magnificence of such study and thought makes the field vibrant, interesting, and far-reaching. The birth of physical cosmology is often considered to be 1929, when Edwin Hubble discovered that the universe is expanding. This was found by observing that the recession velocities of galaxies followed the famous relation now known as Hubble's Law:

$$V = H_0 d \tag{1}$$

where V is the recession velocity, d is the distance to the galaxy, and H_0 is the Hubble constant at the present time. From then on, cosmologists have been constructing models of the universe in accordance with physical observation.

To describe the evolution of our universe we must assume the Cosmological Principle stating the homogeneity and isotropy of the spatial part of spacetime. We then use the famous Einstein field equations describing how the mass-energy of matter curves spacetime:

$$R^{\mu\upsilon} - \frac{1}{2}g^{\mu\upsilon}R + g^{\mu\upsilon}\Lambda = \frac{8\pi G}{c^4}T^{\mu\upsilon} \tag{2}$$

where $R^{\mu\upsilon}$ is the Ricci curvature tensor, R is the Ricci curvature scalar, $g^{\mu\upsilon}$ is the metric tensor, Λ is the cosmological constant, G is Newton's gravitational constant, c is the speed of light in a vacuum, and $T^{\mu\upsilon}$ is the stress-energy tensor. One must note that to be consistent with the homogeneity and isotropy of space, the universe can be modeled as a perfect fluid such that the stress-energy tensor for curved spacetime is:

$$T^{\mu\upsilon} = (\rho + p)u^{\mu}u^{\upsilon} + g^{\mu\upsilon}p \tag{3}$$

where ρ is the density, p is the pressure, and u is the four-velocity of the fluid. Equipped with the proper metric tensor we can begin to explain the evolution of the universe.

This leads us to consider the Freidmann-Lemaitre-Robertson-Walker (FLRW) metric for expanding space as a solution to Einstein's equation:

$$ds^2 = -dt^2 + a^2(t)\left(\frac{dr^2}{1 - kr^2} + r^2(d\theta^2 + sin^2\theta d\phi^2)\right) \tag{4}$$

In the FLRW metric, k is the measure of the curvature of the universe which can take the value 0 for a flat geometry, +1 for an elliptical or closed geometry, and -1 for a hyperbolic or open geometry. We now know through observation that our universe today is spatially flat, corresponding to $k = 0$. The coordinates (t, r, θ, ϕ) describe a spherically symmetric comoving spacetime. The parameter $a(t)$ is the cosmological scale factor which relates a fixed distance r in a comoving coordinate system (necessary for describing the expansion of the universe) to proper distance d by $d = a(t)r$. The scale factor can be related to the cosmological redshift z:

$$a(t) = \frac{1}{1 + z} \tag{5}$$

By solving Einstein's equation for the FLRW metric we can then derive the exalted Freidmann equations (6, 7) describing the evolution of the scale factor through time:

$$\left(\frac{\dot{a}}{a}\right)^2 = \frac{8\pi G}{3}\rho - \frac{kc^2}{a^2} \tag{6}$$

$$\frac{\ddot{a}}{a} = -\frac{4\pi G}{3}\left(\rho + \frac{3p}{c^2}\right) \tag{7}$$

Describing the evolution of the scale factor over cosmological time with the Freidmann equations allows us to elucidate the different constituents of the universe such as matter, radiation and dark energy at distinctive cosmic epochs and explore alluring facts about our universe.

One of the striking features of the Freidmann equations is a singularity when $a(t) = 0$. This singularity is the famed Big Bang: the birth of our universe and the beginning of space and time. When $a(t) = 0$ the curvature of spacetime goes to infinity along with the densities of matter and radiation. The Big Bang occurred at every place in space at one single moment in time. The notion of spacetime completely breaks down at the Big Bang singularity along with Einstein's equation making any predictions in cosmology and physics impossible before or at the Big Bang. Therefore, cosmologists' study of the universe begins with the Big Bang, roughly 13.7 billion years ago (Hartle ch. 18, 22).

1.1.2 Dark Matter

When the Universe was in its infancy, cosmic microwave background (CMB) radiation was coupled with baryonic matter. Early universe density perturbations, which are thought to be the seeds of the large scale structure of the universe, would have been smoothed out by these CMB photons. As the Universe expanded this initial small-scale smoothness would have grown to large scales leaving the universe void of any structure. In short, if baryonic matter was the only form of matter in the universe; galaxies, stars, and planets would never have formed (Loeb 30-34).

In 1970, Vera Rubin and Kent Ford observed the orbital speeds of stars in the galaxy M31. The expected orbital velocity of a star around its galactic center is given by the relation:

$$v = \sqrt{\frac{GM}{R}} \tag{8}$$

where G is the gravitational constant, R is the distance from the galactic center, and M is the mass contained within a sphere of radius R centered at the galactic center. Thus, you expect the relation between orbital speed and orbital radius to be $v \propto 1/\sqrt{R}$. Astonishingly, Rubin and Kent observed motion that was drastically different from Keplerian dynamics; at a large enough radius, orbital velocities of stars stayed roughly constant as radius increased. This was baffling because one would expect these stars to be ejected into interstellar space instead of orbiting the galactic center. This behavior of the non-Keplerian orbital dynamics of stars around galaxies is observed for most galaxies in the Universe. Thus cosmologists deduced that there must be some form of matter surrounding galaxies that provides a sufficient gravitational 'anchor' to avoid these stars from being flung out into intergalactic space. This matter is what is known today as dark matter and the halo surrounding galaxies is the dark matter halo.

There are two theories of dark matter: cold dark matter and hot dark matter. Observations of the large scale structure of the universe indicate that nearly all of the dark matter in the universe is comprised of cold dark matter. Cold dark matter particles might be supersymmetric particles that were non-relativistic at the time they decoupled from other constituents of the Universe. These particles fall under the category of Weakly Interacting Massive Particles (WIMPs), which are heavy enough to be elusive to modern-day collider experiments and only interact with other particles through gravity and possibly the weak nuclear force. Since dark matter does not interact with electromagnetic radiation, dark matter would be 'immune' to the initial smoothing caused by matter-CMB photon coupling in the early Universe discussed before. As a result, the small-scale density perturbations would not have been smoothed allowing for them to expand and grow into the large scale structure of the Universe we observe today. This makes dark matter a necessary ingredient for cosmological models to succeed in explaining the Universe.

In fact, observations from seven-year data release of the Wilkinson Microwave Anisotropy Probe (WMAP 7) show that the density parameters for dark matter and baryonic matter are $\Omega_{dm} = 0.222 \pm 0.026$ and $\Omega_b = 0.0449 \pm 0.0028$ respectively where the density parameter is defined as:

$$\Omega_i \equiv \frac{\rho_i}{\rho_{crit}} \tag{9}$$

and ρ_{crit} is the critical density of the universe at the present time given by:

$$\rho_{crit} = \frac{3H_0^2}{8\pi G} \tag{10}$$

Thus, most of the matter in the universe is comprised of non-baryonic dark matter. Understanding the nature of dark matter and the ways in which dark matter halos form around galaxies and galaxy clusters is an essential ingredient to understanding the large scale structure and evolution of the universe (Ryden ch. 8,12).

For a complete model of cosmology one must also consider the vacuum energy, more commonly known as dark energy. Dark energy, denoted Λ, comprises most of the energy density of the universe today and is considered the perpetrator of the accelerated expansion of the universe. This leads us to the widely accepted and tested cosmological model of the universe, that of a ΛCDM cosmology.

1.1.3 Dark Matter Halos

Dark matter halos provide the nurseries in which galaxies and galaxy clusters form, and are the largest constituents of the large scale structure of the universe. Dark matter halos cannot be observed directly, but their existence can be inferred from their gravitational effects on the rotation curves of galaxies and the observed gravitational lensing effects they beget. If dark matter halos in fact did not exist, this would lead one to conclude the Einstein's Theory of General Relativity describing curved spacetime and gravitational interactions is incorrect.

Through CDM simulations (Allgood et al 2006, Schnieder et al. 2012) and recent weak lensing observations (Hoekstra et al. 2004, Mandelbaum et al. 2005) it has been determined that dark matter halos are non-spherical three-dimensional triaxial ellipsoids. Because most halos possess such an inclination to being non-spherical, it leads one to believe that understanding the shapes of dark matter halos will lead to a better understanding of halo formation and galaxy morphology.

1.2 In This Thesis

This thesis builds on an immense body of work done studying the structure of cold dark matter halos. With recent advancements in N-body cosmological simulations and supercomputing the methods of studying the structure of dark matter halos has evolved. N-body simulations allow for the opportunity to test ΛCDM with unprecedented accuracy and compare a large spectrum of cosmological parameters with observation.

We use the Bolshoi (Klypin et al. 2011) and Multidark (Prada et al. 2011) cosmological simulations enabling us to study the concentration and shape of dark matter halos over six orders of magnitude. Both Bolshoi and Multidark were run on the NASA *Pleides* supercomputer. The halo-finder used in our analysis is the Rockstar Phase-space Temporal Halo Finder (Rockstar; Behroozi et al. 2013). Halo catalogues documenting properties of dark matter halos have been produced by Peter Behroozi and are extensively used in this analysis. Other notable halo finders are Friends-of-friends (FOF; Davis et al. 1985) and Bound Density Maxima (BDM: Klypin et al. 1999), but we restrict this analysis to catalogs computed by Rockstar.

It is interesting to examine how halo concentration $c \equiv \frac{R_{vir}}{R_s}$ changes as a function of mass and evolves over cosmological time (redshift). We define the concentration by using a scale radius found by fitting a Navarro-Frenk-White density profile and a method presented in Prada et al. 2011. The method used in Klypin et al has been shown to be more robust than a fitted scaled radius for halos with 100 particles or less because halo profiles are not well defined for distances on the order of the force resolution of the simulation (Behroozi et al 2013). Recent work has shown that the median concentration steadily decreases with increasing mass and redshift (Bullock et al. 2001). More recently, Klypin et al. 2010 demonstrated that for high redshifts, median concentration starts flat and increases with mass. The most interesting feature of the mass-concentration of halos is we observe the relation to flatten for halo masses $\sim (10^{14} - 10^{15})h^{-1}M_\odot$ (Neto et al. 2007, Prada et al. 2011). Explanations for this non-monotonic behavoir in higher mass halos have been attributed to the tendency for massive galaxy cluster size halos to be out of dynamical equilibrium, thus having lower concentration (Neto et al 2007 and Ludlow et al. 2012). They claim that if we restrict our analysis to only 'relaxed' halos (halos in dynamical equilibrium) the upturn goes away and the mass-concentration relationship behaves monotonically for the entire mass range. We present our results of the mass-concentration relationship by using the same and more restrictive values of the selection criteria for halo relaxation presented by Neto et al. 2007 and later used by Ludlow et al. 2012. One of the goals of this paper is to further examine the effects of restricting our analysis to only halos in dynamical equilibrium.

It has been shown halo shapes become more elliptical and non-spheroidal as mass increases (Allgood et. al 2006, Schnieder et al. 2012). Halo shape in N-body simulations can be recovered from the eigenvalues and eigenvectors of a diagonalized shape tensor (Zemp et al. 2011) or diagonalized weighted inertia tensor (Allgood et al. 2006). Past work has shown (Dubinski & Carlberg 1991, Jing & Suto 2002, Allgood et al. 2006) have found that the mean shape of halos is highly correlated to mass. We compare these two common methods for calculating dark matter halo shape. In addition, we compare these two methods at two different halo radii R_{vir} and $0.3R_{vir}$. Motivation for measuring the shape at $0.3R_{vir}$ is that most halos should be in virial equilibrium at this radii. In addition, X-ray gas observation get noisier as the distance from the center of a halo increases so for comparison with observations we measure the shape at $0.3R_{vir}$.

Section 2 of this thesis discusses the simulations, halo-finders, and halo catalogues used in this work. In section 3 we present results for the mass-concentration relationship of dark matter halos and the effects of halo selection criteria on concentration. In section 4 we present our results for calculating halo shape using two different methods at two different radii. We summarize and discuss the main results of this thesis in section 5.

2 Simulations

Cosmological N-body simulations such as Bolshoi, MultiDark, and Millennium (Springel et al. 2005) allows us to test the predictions of a ΛCDM cosmology with unprecedented accuracy. More specifically, we can study dark matter halo concentrations and shapes over six orders of magnitude of halo mass to encompass in our analysis galaxy sized halos and galaxy-cluster sized halos. Parameters for these simulations are given in Table 1.

2.1 Numerical Simulations

The Bolshoi and MultiDark simulations use cosmological parameters from the five-year and seven-year WMAP data release results. See table 1 for these parameters. The Adaptive-Refinement-Tree (ART) code was used for Bolshoi and MultiDark, where ART is an Adaptive-Mesh-Refinement (AMR) algorithm. For more detailed descriptions of the code please refer to Kravstov et al. 1997 and Kravstov 1999. For details of the Bolshoi simulation refer to Klypin et al. 2010.

The mass of each particle in the Bolshoi and MultiDark simulation are: $1.35{\cdot}10^8 h^{-1} M_\odot$ and $8.63{\cdot}10^9 h^{-1} M_\odot$ respectively. Our analysis ranges from halos of mass $\sim (10^{11} - 10^{15}) h^{-1} M_\odot$, so we expect smallest halos to have roughly a thousand bound particles and largest halos to have roughly a million bound particles.

Table 1: Parameters for ΛCDM cosmological simulations. L_{box} is the length of one side of the simulation, N_p is the number of particles in the simulations, ϵ is the force resolution in a comoving (constant in time) coordinate system, M_p is the mass resolution (mass of each particle). The cosmological density parameters for the simulations are: Ω_m, Ω_b, Ω_Λ. The spectral index of the primordial power spectrum is n_s, h is the Hubble constant at the present time in units of 100 $km/sMpc^{-1}$ and σ_8 is the amplitude of mass density fluctuations of spheres of 8 $Mpch^{-1}$ at redshift z=0. Millennium parameters from Springel et al. 2005, Millennium-II parameters from Boylan-Kochlin et al. 2009, Bolshoi parameters from Klypin et al. 2009 and MultiDark parameters from Prada et al. 2011

Name	L_{box} (h^{-1}Mpc)	N_p	ϵ (h^{-1}kpc)	M_p ($h^{-1}M_\odot$)	Ω_m	Ω_Λ	n_s	h	σ_8
Millennium	500	2160^3	5	$8.61{\cdot}10^8$	0.25	0.75	1.00	0.73	0.90
Millenium-II	100	2160^3	1	$6.89{\cdot}10^6$	0.25	0.75	1.00	0.73	0.90
Bolshoi	250	2048^3	1	$1.35 \cdot 10^8$	0.27	0.73	0.95	0.70	0.82
MultiDark	1000	2048^3	7	$8.63 \cdot 10^9$	0.27	0.73	0.95	0.70	0.82

2.1.1 Halo Finder

The main data sets used for the analysis of large cosmological simulations are halo catalogues. Halo catalogues contain all the relevant intrinsic properties such as position, angular momentum, mass and axial ratios needed for detailed analysis. Dark matter halos for Bolshoi and MultiDark simulations have been identified using the Rockstar Halo Finder (Behroozi et al. 2013).

Rockstar starts by dividing the simulation volume into 3D Friends-of-Friends (Davis et al. 1985; hereafter FOF) groups for parallelization ease. Then a phase metric is found be dividing particle positions and velocities by the group position and velocity dispersions. A phase-space linking length is then chosen such that 70% of each groups particles are linked together in sub groups. This process repeats for new linking-lengths and substructure. Upon all grades of substructure being identified particles are assigned to the nearest halo in phase space. Once all particles have been assigned to halos unbound particles are removed from halos (Behroozi et al. 2013).

3 Halo Concentration

The Navarro-Frenk-White (1995, 1996, 1997; hereafter NFW) density profile describing the density as a function of radius for dark matter halos is given by:

$$\rho_{nfw} = \frac{4\rho_s}{\frac{r}{r_s}(1+\frac{r}{r_s})^2} \tag{11}$$

Here r_s and ρ_s are the scale radius and density respectively, where the scale radius is the radius between an inner r^{-1} density profile and an outer r^{-3} profile (Prada et al. 2011). The NFW profile is a useful tool for fitting halo density profiles of bound particles in simulations. Remarkably, the NFW profile tends to hold for all halos that have been assembled in a hierarchical manner and are approaching virial equilibrium, with little dependence on the specifics of the cosmological model (Neto et al. 2007).

One of the parameters, ρ_s or r_s, in the NFW profile can be replaced by a virial parameter (M_{vir}, R_{vir}, V_{vir}) or a parameter at two hundred times the critical density of the universe (M_{200}, R_{200}, V_{200}) where R is the radius, M is the mass and V is the circular velocity. The virial radius of a halo can then be defined as the radius of a sphere such that:

$$M_{vir} = \frac{4\pi}{3}\Delta_{vir}\rho_{cr}(z)R_{vir}^3 \tag{12}$$

and the radius at two hundred times the critical density can be defined:

$$M_{200} = \frac{4\pi}{3}\Delta_{200}\rho_{cr}(z)R_{200}^3 \tag{13}$$

where $\rho_{cr}(z)$ as the critical density of the universe as a function of redshift and the overdensity Δ is:

$$\Delta(z) = 18\pi^2 + 82(\Omega_m(z) - 1) - 39(\Omega_m(z) - 1)^2 \tag{14}$$

$$c_{vir} = \frac{R_{vir}}{r_s} \tag{15}$$

$$c_{200} = \frac{R_{200}}{r_s} \tag{16}$$

We define the halo concentration $c = \frac{R_{vir}}{r_s}$ using two different methods to calculate the scale radius. The first method, divides halo particles into a maximum of 50 radial mass bins of equal size with no less that 15 particles per bin (Behroozi et al. 2013) and a NFW profile is used to determine the best fit for the scale radius. Figure 1 shows the concentration-mass relationship using this definition of the scale radius.

The second method to calculate the scale radius (Klypin et al. 2011) uses the maximum circular velocity V_{max} and the circular velocity at the virial radius and notes that these (and any two other independent quantities) can be used to estimate the concentration. The velocity ratio:

$$V_{max}\sqrt{\frac{R_{vir}}{GM_{vir}}} \tag{17}$$

can be used to estimate the halo concentration regardless of the halo density profile, but for the case of the NFW profile the velocity ratio is given in Klypin et al. 2011 by:

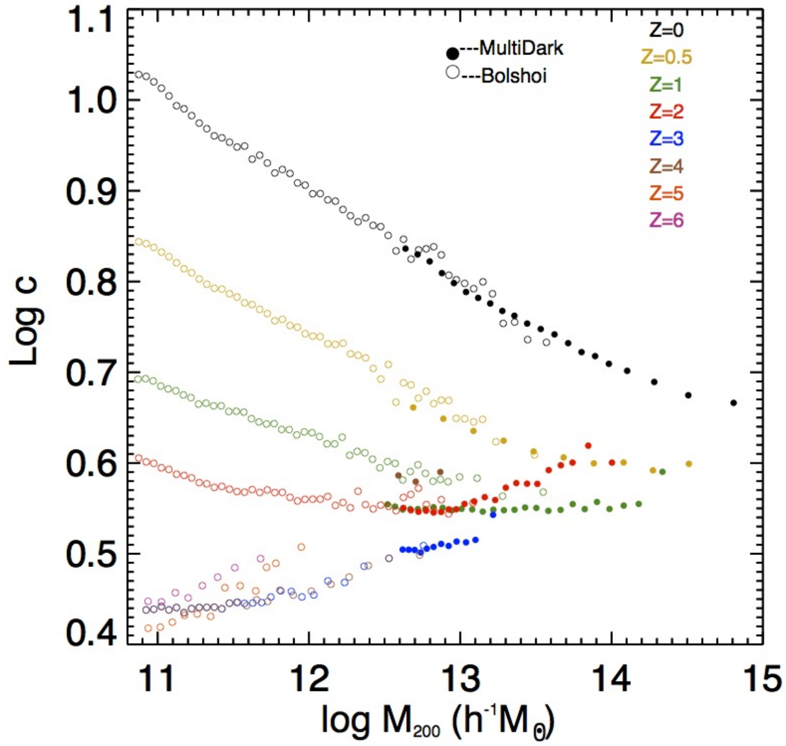

Figure 1: Halo mass-concentration relation for distinct halos for Bolshoi (open symbols) and Multidark (filled symbols) the NFW fitted scale radius.

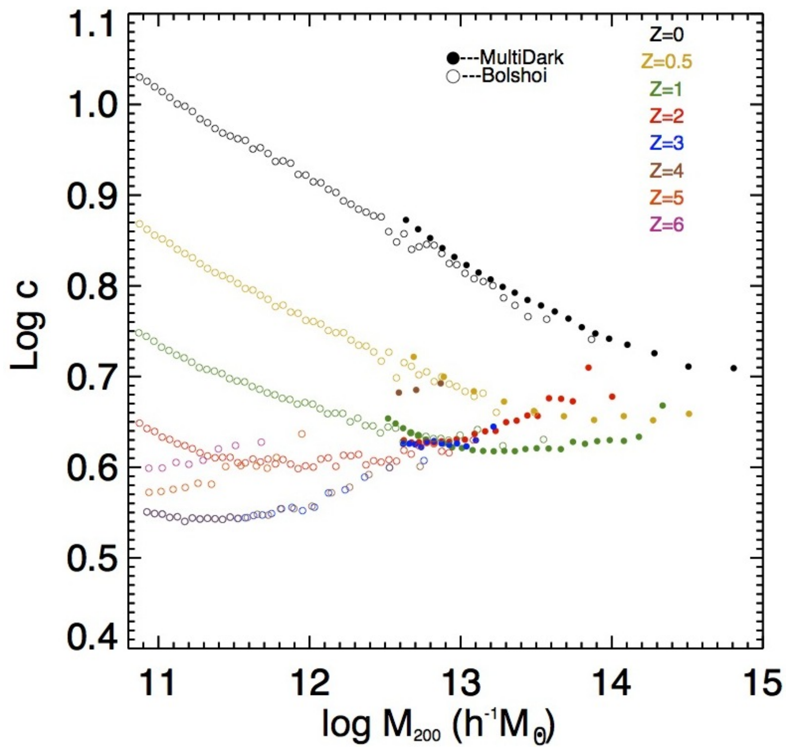

Figure 2: Halo mass-concentration relation for distinct halos for Bolshoi (open symbols) and Multidark (filled symbols) using the Klypin scale radius.

$$V_{max}\sqrt{\frac{R_{vir}}{GM_{vir}}} = \left(\frac{0.216c}{f(c)}\right) \tag{18}$$

where $f(c)$ is:

$$f(c) \equiv \ln(1+c) - \frac{c}{1+c} \tag{19}$$

Since we already have the virial ratio for each halo, equations 18-19 are solved numerically to get the concentration $c = \frac{R_{vir}}{r_s}$. We then can easily derive the scale radius, which we call the Klypin scale radius. The concentration used plotting the Klypin scale radius is showing in Figure 2.

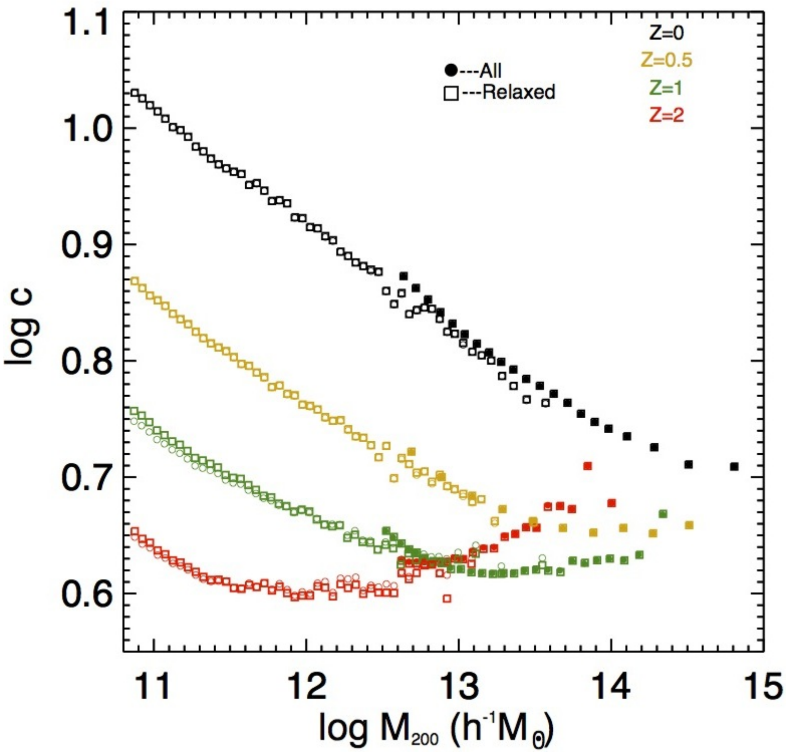

Figure 3: Halo mass-concentration comparison between all the halos and the relaxed sample. The relaxation criteria in this figure is κ <1.3. Squares represent the relaxed samples and circles represent the whole simulation. Bolshoi is open symbols and Multidark is closed symbols. There is essentially no change in the relaxed sample so data point are appear over plotted.

For both methods of defining the concentration we see the concentration flatten for higher mass halos and as redshift increases. We see a strong upturn from redshift z=2 and higher. The concentration defined by the Klypin scale radius is systematically higher than for the NFW fitted scale radius for all redshifts and mass ranges. Using the NFW fitted scale radius we observe a much steeper upturn for redshifts z=3-6.

3.1 Effects of Selection Criteria on Halo Concentration

Neto et al. 2007 states that because dark matter halos are structures that are constantly evolving due to mass accretion, a large subset of halos tend to be out of virial equilibrium.

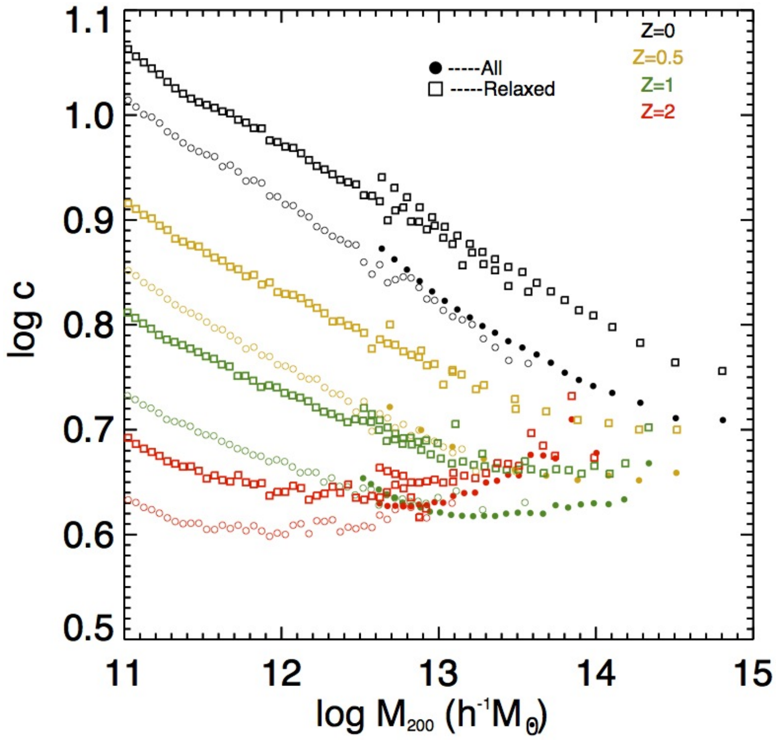

Figure 4: Halo mass-concentration comparison between all the halos and the relaxed sample. The relaxation criteria in this figure is x_{off} <0.07. Squares represent the relaxed samples and circles represent the whole simulation. Bolshoi is open symbols and Multidark is closed symbols.

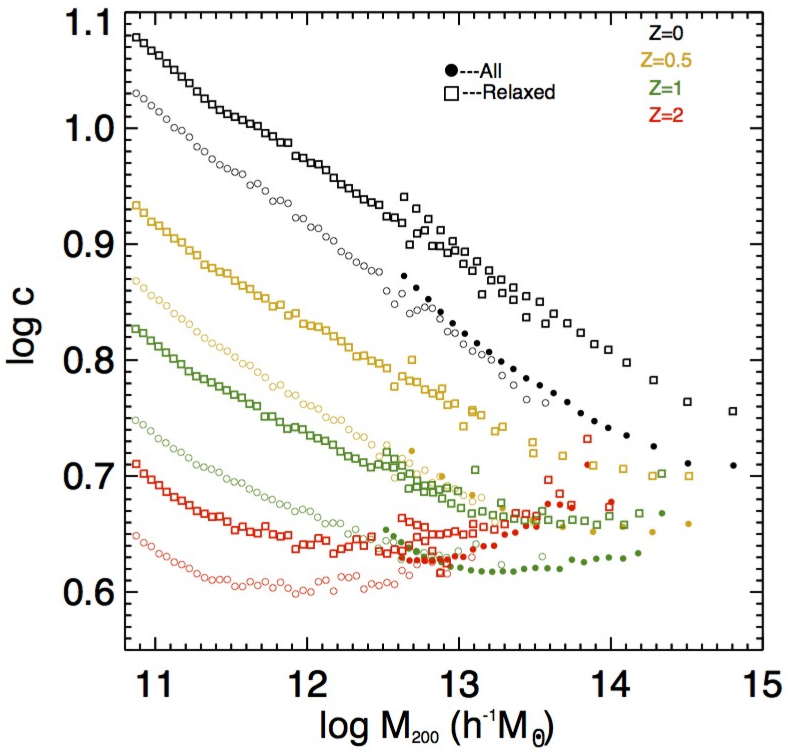

Figure 5: Halo mass-concentration comparison between all the halos and the relaxed sample. Both relaxation criteria are used where κ <1.3 and x_{off} <0.07. Squares represent the relaxed samples and circles represent the whole simulation. Bolshoi is open symbols and Multidark is closed symbols.

In addition, because many large halos are undergoing major mergers the tend to have poorly defined centers making spherically defined density profiles not as useful. Recent results (Neto et al. 2007, Ludlow et al. 2012) have found that if we reduce our analysis to only halos in dynamical equilibrium (relaxed halos), the upturn and flattening in concentration shown in Figures 1-2 disappears. We use the following two objective criteria (Maccio et al. 2008 and Neto et al. 2007) to define a halo has relaxed:

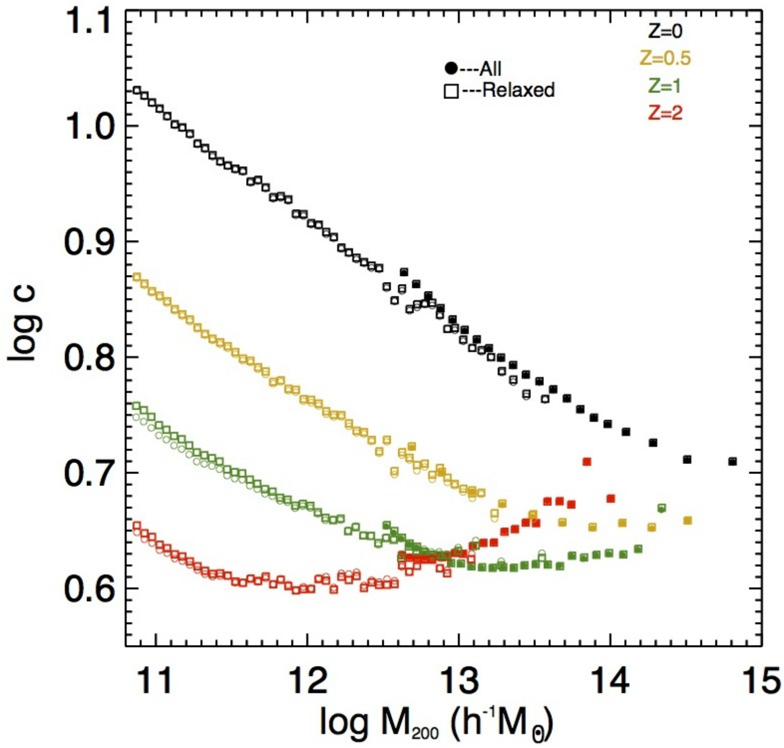

Figure 6: Halo mass-concentration comparison between all the halos and the relaxed sample. The relaxation criteria in this figure is κ <1.1. Squares represent the relaxed samples and circles represent the whole simulation. Bolshoi is open symbols and Multidark is closed symbols.

(i) Offset Parameter: The offset parameter, x_{off} for each halo is defined as the distance from the particle used as the center of the spherical density profile (potential center), R_p, and the center of mass of the halo, R_{cm}, and normalized by the virial radius:

$$x_{off} = \frac{|R_p - R_{cm}|}{R_{vir}} \tag{20}$$

Halos that fall into the relaxation criteria will be radially symmetric and have a low values of x_{off} while halos which are unrelaxed, possibly due to a recent merger, will have asymmetric mass distributions and larger values of x_{off} (Maccio et al. 2008). We test the values x_{off} <0.07 and x_{off} <0.035 for our 'relaxed' samples.

(ii) Virial Ratio: The virial ratio (Maccio et al. 2003), which we will denote κ, is a kinematical property of a dark matter halo. We use kinetic energy and potential

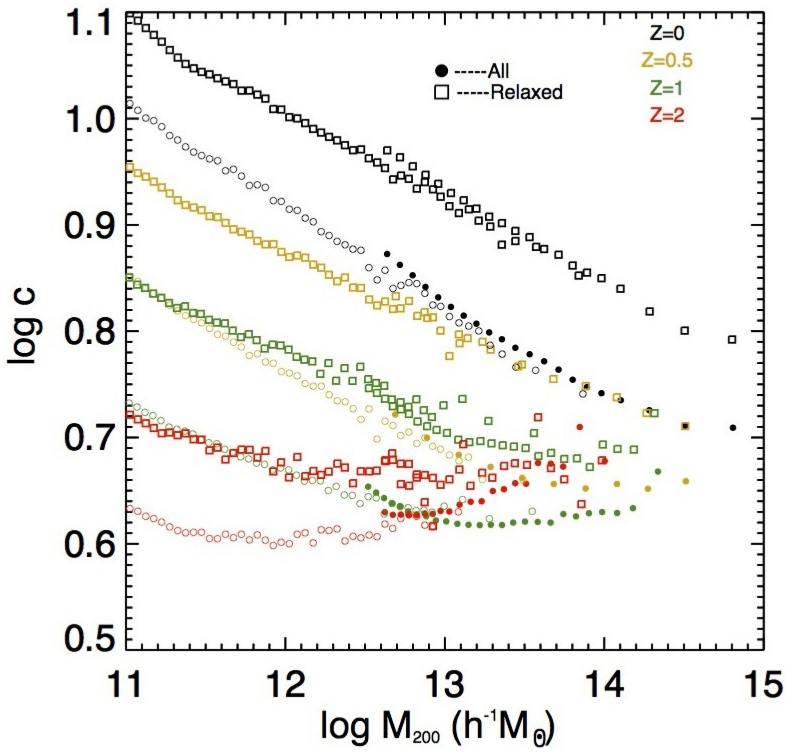

Figure 7: Halo mass-concentration comparison between all the halos and the relaxed sample. The relaxation criteria in this figure is x_{off} <0.035. Squares represent the relaxed samples and circles represent the whole simulation. Bolshoi is open symbols and Multidark is closed symbols.

energies of all the particles within the virial radius to define the virial ratio as follows:

$$\kappa = \frac{\displaystyle\sum_{i(r_i<r)} mv_i^2}{\left| -\displaystyle\sum_{i<j(r_{i,j}<r)} \frac{Gm^2}{r_{ij}} \right|} = \frac{2T(< R_{vir})}{|-W(< R_{vir})|} \tag{21}$$

We test the values of κ <1.3 and $\kappa < 1.1$ in this paper.

We impose the relaxation criteria: κ <1.3, x_{off} <0.07 and then both together – shown in figures 3, 4, 5 respectively. These values correspond to those used in Neto et al. 2007 and Ludlow et al. 2011. We see little change in the concentration by restricting the kinematical quantity κ <1.3. It is evident that we do not see a tendency towards a more monotonic behavior for halo concentration by restricting our halo samples, but we do see a systematic increase in concentration for z=0,0.5,1,2 when x_{off} <0.07. At redshift z=2, we observe the concentrations of the relaxed sample (x_{off} <0.07) converging with the values of our sample containing all halos. By restricting both x_{off} <0.07 and κ <1.3 the concentration systematically rises, but there is no evidence of the upturn disappearing. The relaxation criteria x_{off} has a much more dramatic effect on the concentration than κ, which is virtually negligible.

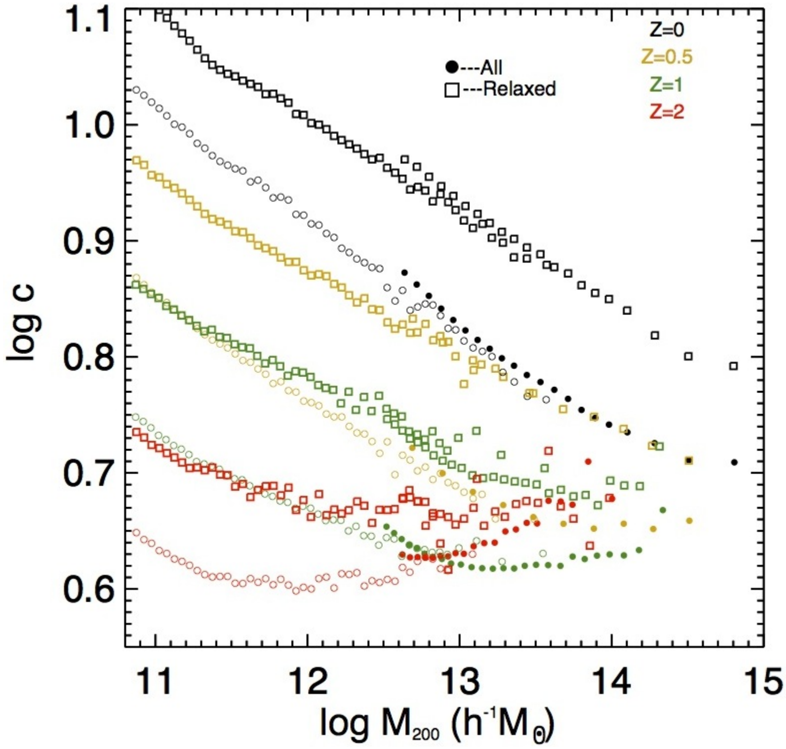

Figure 8: Halo mass-concentration comparison between all the halos and the relaxed sample. Both relaxation criteria are used where κ <1.1 and x_{off} <0.035. Squares represent the relaxed samples and circles represent the whole simulation. Bolshoi is close symbols and Multidark is closed symbols.

Next we impose more selective relaxation criteria: κ <1.1, x_{off} <0.035 and then both together – shown in figures 6, 7, 8 respectively. Restricting our halo sample to halos with κ <1.1 (Figure 6) has very little effect on the concentration-mass relation. We do observe a small drop in concentration for redshifts z=1,2. If we only sample halos with x_{off} <0.035 (Figure 7) we see a systematic increase in the concentration for all redshifts. At redshifts z=1,2 we observe the concentrations of our relaxed samples (x_{off} <0.035) converge with the values of our sample containing all halos. If we impose both criteria (Figure 8), x_{off} <0.035 and κ <1.1, we see the concentration rise significantly more than just restricting x_{off} <0.035 (Figure 7).

The percentage of halos which pass our tests for relaxation changes with redshift and mass. In Figure 9 and 10 we plot the percentage of halos in each bin which pass a given relaxation criteria. A low percentage (ratio) implies that there are very few relaxed halos in this bin. Massive halos are more likely to be unrelaxed than less massive halos for a given redshift as Figure 9-10 suggest. As redshift increases, the percentage of relaxed halos in a given bin drops significantly. We plot the ratio of relaxed halos to the total number of halos in a mass bin for the relaxation criteria: x_{off} <0.07 (Figure 9) and x_{off} <0.035 (Figure 10). We observe resolution effects for halos with less than 5000 particles: for Bolshoi this is for halos with $M \leq 6.75 \cdot 10^11 h^{-1} M_{\odot}$ and Multidark $M \leq 4.32 \cdot 10^13 h^{-1} M_{\odot}$. Vertical lines are drawn for both Bolshoi and Multidark where N_p =5000 in Figure 9 and Figure 10. We do not plot the ratio for our restrictions of κ

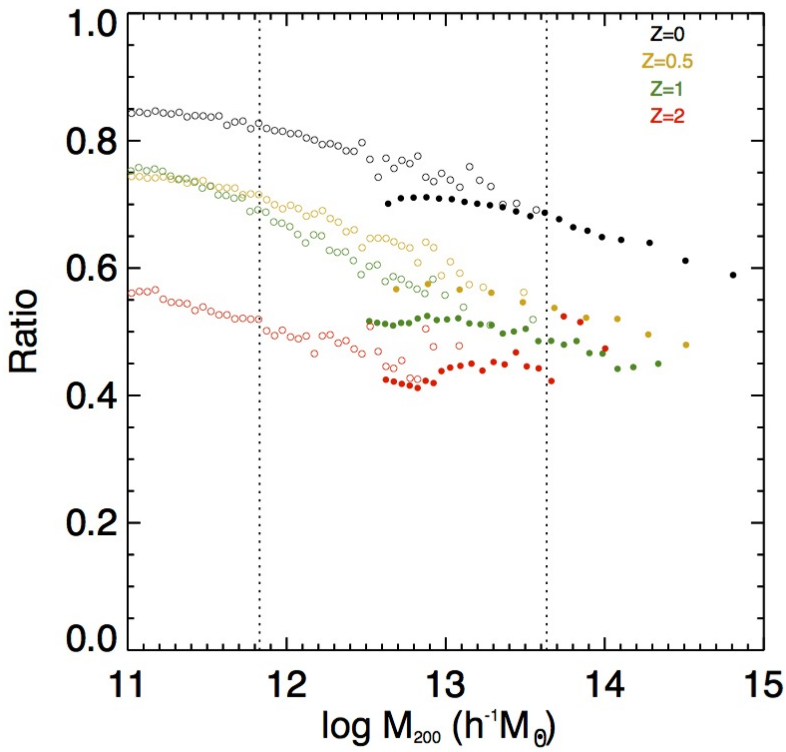

Figure 9: Percentage of relaxed halos (x_{off} <0.07) for a given mass bin. Lines are drawn at N_p =5000 for Bolshoi and Multidark. Bolshoi is open symbols and Multidark is closed symbols.

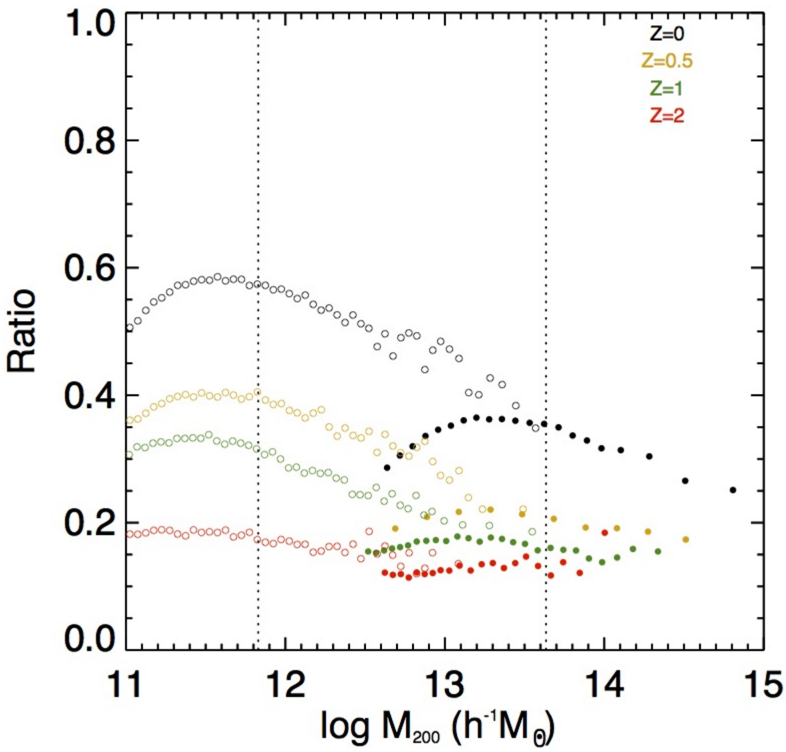

Figure 10: Percentage of relaxed halos (x_{off} <0.035) for a given mass bin. Lines are drawn at N_p =5000 for Bolshoi and Multidark. Bolshoi is open symbols and Multidark is closed symbols.

because nearly all halos in th bins satisfy the criteria.

4 Dark Matter Halo Shapes

We investigate the shapes of dark matter halos for the Bolshoi and MultiDark simulations. To begin exploring dark matter halo shapes we name the three principal axes of dark matter halos a, b, and c and use the following definitions to determine axial ratios (Allgood et. al 2006):

$$s = \frac{c}{a},\ p = \frac{c}{b},\ q = \frac{b}{a} \tag{22}$$

Ellipsoids are characterized in three classes corresponding to their axial ratio ranges: prolate ellipsoids with axial ratios $s \approx q < p$, oblate ellipsoids with axial ratios $s \approx p < q$, and triaxial ellipsoids where all three principal axes have different lengths and generally follow $a > b > c$. It has been shown the the median axis ratio $< s >$ increases as a function of radius as one moves out farther radii for a given halo and also that cluster sized halos tend to be more aspherical than galaxy size halos (Allgood et al. 2006). Peter Behoorizi has calculated the shape using a method prescribed by Zemp et al. 2011 and another by Allgood et al. 2006 which we compare.

4.1 Shape Calculation - Allgood et al. 2006

The ellipticity of halos can be found by using eigenvectors and eigenvalues from a diagonalized inertia tensor. The eigenvectors will correspond to the direction of the principal axes in space and the eigenvalues will correspond to the axial ratios s, p, q defined previously. The inertia tensor used is a weighted inertia tensor:

$$\tilde{I}_{ij} = \sum_n \frac{x_{i,n} x_{j,n}}{r_n^2} \tag{23}$$

where

$$r_n = \sqrt{x_n^2 + \frac{y_n^2}{q^2} + \frac{z_n^2}{s^2}} \tag{24}$$

is the elliptical distance to the n-th particle in an eigenvector coordinate system. The eigenvalues $(\lambda_a, \lambda_b, \lambda_c)$ allow us to determine the axial ratios s, q, p where the principal axes are $(a, b, c) = \sqrt{\lambda_a, \lambda_b, \lambda_c}$.

This method starts by determining the inertia tensor with $s = q = 1$, a sphere, and including all particles within some determined radius. The initia inertia tensor is deformed along the eigenvectors while keeping the the longest eigenvector constant at the original spherical radius through iterations. The eigenvalues of the inertia tensor are rescaled by:

$$\frac{r_{sph}}{(abc)^{\frac{1}{3}}} \tag{25}$$

where r_{sph} is the initial spherical radius. After each iteration, if particles are no longer within the boundary of the halo they are discarded and particles now within the boundary of the halo are included in the subsequent iteration. We repeat this process until the variance of s and q between iterations is less then some predetermined tolerance (Allgood et al. 2006, Schneider et al 2012). Motivation for weighting the inertia tensor (eq. 23) by the elliptical radius (eq. 24) is to give particles at larger radii less weight. Substructure is not removed.

4.1.1 Shape at R_{vir}

4.1.2 Shape at $0.3R_{vir}$

4.2 Shape Calculation - Zemp et al. 2011

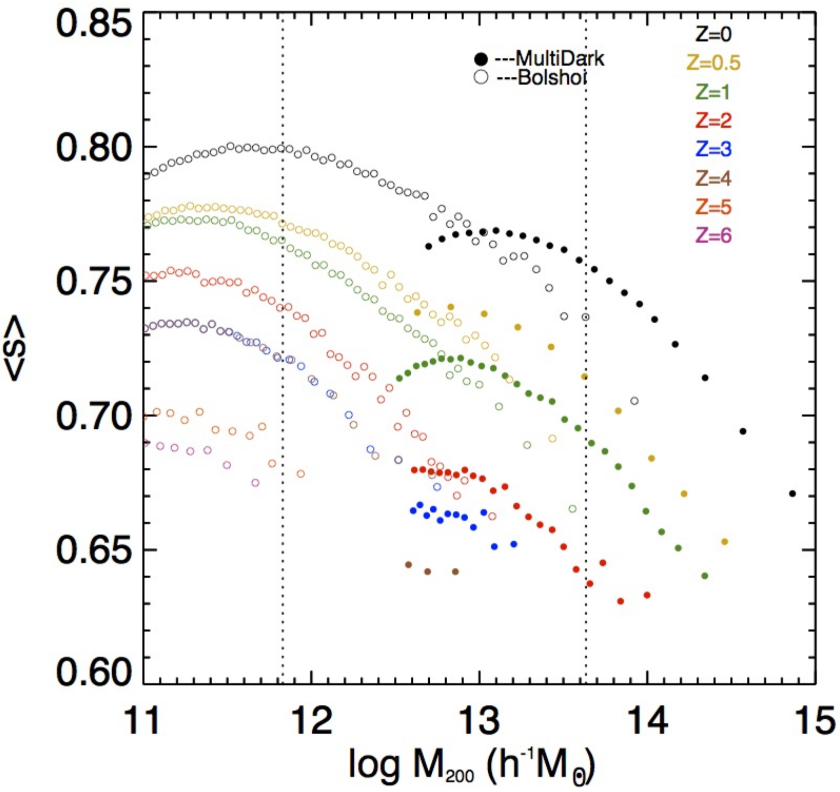

Figure 11: Median axis ratio at R_{vir} using the Zemp et al. 2011 method. Due to resolutiong effects in calculating the shape we indicate where N_p =5000 for Bolshoi and Multidark. Bolshoi is open symbols and Multidark is closed symbols.

Peter Behroozi has also calculated halo shapes using a form of the Zemp et al. 2011 perscription in his Rockstar halo catalogs. As mentioned before, immense motivation for this analysis is held in the method which halo shapes are determined.

$$S_{ij} = \frac{\sum_n m_n x_{i,n} x_{j,n}}{\sum_n m_n} \tag{26}$$

Here m_n is the mass and $x_{i,n}$ is $i-$th component of the position vector of the n-th particle with the summation being done over all particles within the integration volume. A weight function can be added such that:

$$S_{ij} = \sum_n \frac{w(\mathbf{x}) m_n x_{i,n} x_{j,n}}{m_n} \tag{27}$$

where $w(\mathbf{x})$ is the weight function dependent on the position vector $\mathbf{x}$ with respect to the center of the halo. It must be noted that if $w(\mathbf{x}) = r_n^{-2}$, we recover equation 23. The Rockstar catalogues use $w(\mathbf{x})$=1. The weight function and its effect on the shapes of halos is discussed extensively in Zemp et al. 2011.

The calculation of shape starts by using a spherically symmetric volume. The shape tensor S is diagonalized and we recover the eigenvectors and eigenvalues. As before, the eigenvectors give the directions of the principal axes and the ratio of the eigenvalues allows us to determine the axial ratios s, p, q. The longest principal axis is kept equal to the initial spherical virial radius for all iterations, but is able to rotate freely in space. Then S is calculated again summing over all particles within the new deformed integration volume. This iterative process continues until convergence is reached and we have recovered the triaxial ellipsoid shape. All substructure is excluded in the calculation (Zemp et al 2011).

4.2.1 Shape at R_{vir}

4.2.2 Shape at 0.3R_{vir}

For more detailed discussion on determining shapes of dark matter halos please refer to Dubinski & Carlberg 1991, Jing & Suto 2002, Allgood et al. 2006, Zemp et al. 2011 and Schneider et al. 2012. For discussion of the iteration method refer to Katz 1991, Dubinski & Carlberg 1991, and Warren et al. 1992.

5 Summary and Discussion

References

[1] Allgood, B., Flores, A. F., Primack, J. R., Kravstov,V. A., Wechsler, H. R., Faltenbacker, A., Bullock, J. S., 2006, MNRAS, 367, 1781A

[2] Behroozi, P. S., Wechsler, R. H., Wu, H., 2013, ApJ. 762, 109B

[3] Boylan-Kochlin, M., Springel, V., White, S. D.M., Jenkins, A., Lemson, G., 2009, MNRAS, 398, 1150

[4] Bullock, J. S., Kolatt, T. S., Sigad, Y., Somerville, R. S., Kravtsov, A. V., Klypin, A. A., Primack, J. R., Dekel, A., 2001, MNRAS, 321, 559

[5] Davis, M., Efstathiou, G., Frenk, C. S., White, S. D.M., 1985, ApJ, 292, 371

[6] Dubinski, J., Carlberg, R. G., 1991, ApJ. 378, 496D

[7] Hahn, O., Cristiani, P., Carolo, C. M., Dekel, A., 2009, MNRAS, 398, 1742H

[8] Hahn, O., Teyssier, R. & Carollo, C. M., 2010, arXiv, arXiv:1002.1964

[9] Hartle, B. J., 2003. *Gravity: An Introduction to Einstein's General Relativity.* Addison Wesley Publishing, San Francisco, California

[10] Jing, Y. P., Suto, Y., 2002, ApJ 574:538-533

[11] Katz, N., 1991, ApJ, 574, 538

[12] Klypin A. A., Holtzman, J., 1997, astro, arXiv:astro-ph/9712217

[13] Klypin, A. A., Trujillo-Gomez, S., Primack, J. R., 2011, ApJ, 740, 102K

[14] Loeb, A., 2010. *How Did the First Stars and Galaxies Form?.* Princeton University Press, Princeton, New Jersey.

[15] Ludlow, A. D. 2002, Ph.D. Thesis

[16] Ludlow, A. D., Navarro, J. F., Li, M., Angulo, R. E., Boylan-Kochlin, M., Bett, P. E, 2012, arXiv:1206.1049v1

[17] Maccia, V. A, Dutton, A. A., van den Bosch, F. C., 2008, arXiv, arXiv:0805.1926v2

[18] Navarro, J. F., Frenk, C. S., White, S. D.M., 1997, ApJ, 490, 493

[19] Neto, A. F., Gao, L., Bett, P., Cole, S., Navaroo, J. F., Frenk, C. S., White, S. D.M., Springel, V., Jenkins, A, 2007, arXiv, arXiv:0706.2919v1

[20] Novak, G.S., Cox, T.J., Primack, J.R., Jonsson, P. & Dekel, A., 2006, arXiv, arXiv:astro-ph/0604121

[21] Prada, F., Klypin, A. A., Cuesta, A. J, Betancort-Rijo, J. E., Primack, J. R., 2012, MNRAS, 423, 3018P

[22] Rieve, K., Partl, A.M., Enke, H., Forero-Romero, J., Gottloeber, S., Klypin, A., Lemson, G., Prada, F., Primack, J. R., Steinmetz, M., Turchaninov, V., 2011, arXiv:1009.0003v2.

[23] Ryden, B. 2006. *Introduction to Cosmology*. Ohio State University Department of Astronomy, Ohio.

[24] Schnieder, D. M., Frenk, S. C., Cole, S., 2012, arXiv, arXiv:1111.5616v2

[25] Springel V., et al., 2005, Nature, 435, 629

[26] Tormen, G., Bouchet, F.R. & White, S. D.M., 1996, arXiv, arXiv:astro-ph/9603132

[27] Trujillo-Gomez, S., Klypin, A., Primack, J.R., Romanowsky, J. A., 2011, ApJ, 742, 16T

[28] Warren, M. S., Quinn, P. J., Salmon J. K., Zurek W. H., 1992, ApJ, 399, 405

[29] Zemp, M., Gnedin O. Y., Gnedin, N. Y., Kravstrov, A. V., 2011, ApJS, 197, 30Z

6 To Do List

1. Analysis for Bolshoi-Planck (?)
2. Compare mass-concentration relation for galaxy cluster sized halos with observational estimates from X-ray (Ettori et al 2010) and kinematic(Wojtak& Lokas 2010) data
3. Conclusion & Acknowledgments